ACS Catalysis

Research Article

pubs.acs.org/acscatalysis

Well-Defined Supported Mononuclear Tungsten Oxo Species as Olefin Metathesis Pre-Catalysts

Yassine Bouhoute,[†] Anthony Garron,[†] Denys Grekov,[‡] Nicolas Merle,[†] Kai C. Szeto,[†] Aimery De Mallmann,[†] Iker Del Rosal,[⊥] Laurent Maron,*[,⊥] Guillaume Girard,[‡] Régis M. Gauvin,*[,‡] Laurent Delevoye,*[,‡] and Mostafa Taoufik*[,†]

[†]Laboratoire de Chimie, Catalyse, Polymères et Procédés, UMR 5265 CNRS, UCBL, ESCPE Lyon, 43 Boulevard du 11 Novembre 1918, F-69616 Villeurbanne Cedex, France

[‡]Unité de Catalyse et de Chimie du Solide, CNRS UMR 8181, Université de Lille, F-59655 Villeneuve d'Ascq, France

[⊥]Laboratoire de Physico-Chimie des Nano-Objets, CNRS UMR 5215, Université de Toulouse, INSA, UPS, 135 Avenue de Rangueil, F-31077 Toulouse, France

Supporting Information

ABSTRACT: $[WOCl_4]$ was grafted on silica dehydroxylated at 200 °C, and the structure of the surface species was elucidated by a combination of spectroscopic and theoretical methods, demonstrating the formation of $[(\equiv SiO)_2WOCl_2]$ (**1a**) as the major species accompanied by minor monopodal species $[(\equiv SiO)WOCl_3]$ (**1b**). Most noteworthy, EXAFS and ^{17}O NMR combined to DFT calculations helped elucidate the structure of the surface species. Alkylation was performed using $SnMe_4$, affording methyl species that were also precisely characterized. The alkylated species achieved excellent performances in isobutene metathesis to 2,3-dimethylbutene.

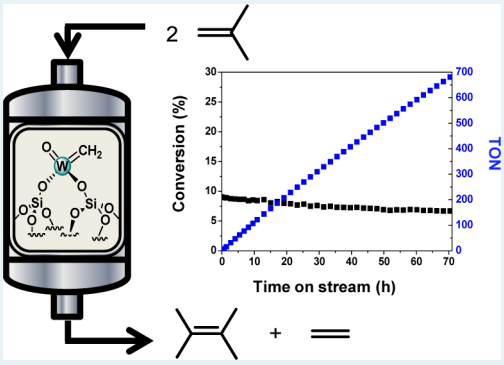

KEYWORDS: *metathesis, surface chemistry, tungsten, tin, alkylation*

INTRODUCTION

Olefin metathesis is a reaction of major industrial importance.[1] The most widely used type of catalyst is WO_3 deposited on an inorganic support such as silica. In this case, it has been proposed that the active sites are bipodal high valent carbene species.[2,3] Using surface organometallic chemistry approach,[4] we developed the first example of well-defined (monopodal) oxo alkyl species that performed efficiently in olefin metathesis, as a step further toward the development of model species for the WO_3/SiO_2 active sites.[5] Several years later, this approach was also explored by others,[6] generating organometallic surface species singly bound to the support through a siloxide moiety. However, concerns arose, regarding, for example, the lack of selectivity of the grafting and/or arduous synthesis of molecular organometallic precursors.

We reasoned that cleavage of the metal−chlorine bond can be a more convenient entry into the anchoring of mononuclear centers onto an inorganic support. This was shown for $[WOR_3Cl]$, where the W−Cl was selectively cleaved to afford $[(\equiv SiO)WOR_3]$ species (with R = CH_2tBu).[7] Along the same line, previous examples for the grafting of transition metal chlorides afforded well-defined surface species, as in the case of $[VOCl_3]$,[8] $[CrO_2Cl_2]$[9] or $[TiCl_4]$.[10] The resulting chloride species could then be alkylated and thus afford tungsten alkyl species through a more practical way than grafting of sensitive and expensive organometallics. An early example of such reactivity was provided by Mol, who used $SnMe_4$ as an activator of $[WOCl_4]$ to trigger metathesis activity.[11] On the basis of these premises, we set out to study the grafting of $[WOCl_4]$ under controlled conditions. We selected silica dehydroxylated at 200 °C as the support, as it mostly bears vicinal silanols that have been reported to favor the formation of bipodal species.[12] The alkylation of this grafted complex is then studied, targeting $[(\equiv SiO)_2W(CH_3)_2]$, closely related to the active species proposed in the case of the WO_3/SiO_2 industrial catalyst.[2] The modification of coordination sphere of W is followed step by step through chemical and spectroscopic characterizations (mass balance analysis, ^{17}O and ^{13}C NMR with labeled compounds, IR, EXAFS) supported by DFT calculations.

RESULTS AND DISCUSSION

Grafting of $[WOCl_4]$ on SiO_{2-200}. The grafting of $[WOCl_4]$ on SiO_{2-200} was carried out by a mechanical mixing at 80 °C. After 3 h, volatile compounds were condensed into an

Received: August 29, 2014
Revised: October 17, 2014
Published: October 17, 2014

   dx.doi.org/10.1021/cs501294j | ACS Catal. 2014, 4, 4232−4241

infrared cell (of known volume) in order to quantify HCl evolved during grafting by infrared spectroscopy[7] and to establish the mass balance of the reaction. Then, the powder was washed three times with toluene in order to remove the excess of $[WOCl_4]$ and finally rinsed with dry pentane to remove any physisorbed toluene, affording **$WOCl_4$-SiO_{2-200}** as a pale yellow material. The reaction of $[WOCl_4]$ proceeds with consumption of almost all free surface silanols of SiO_{2-200}, as shown from the irreversible disappearance of the silanol stretching band at 3747 cm^{-1}. (Figure 1).

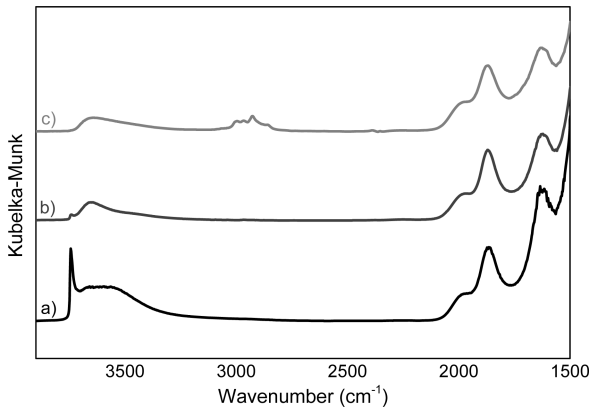

Figure 1. DRIFT spectra of SiO_{2-200} (a); **$WOCl_4$-SiO_{2-200}** (b); **WOMe-SiO_{2-200}** (c).

The amount of W and Cl, as quantified by elemental analysis of **$WOCl_4$-SiO_{2-200}** are 7.26 and 3.13 wt %, respectively, which accounts for 2.22 Cl/W. On the other hand, 0.396 mmol of W/g of silica is grafted, although the concentration of silanols is about 0.86 mmol OH/g[13] on SiO_{2-200}, which amounts to a W/OH ratio of 0.46. Quantification of gas evolved during the grafting (by integrating the ν(H−Cl) and by comparing to a calibration curve) showed that 1.7 HCl/W are released. The results obtained with SiO_{2-200} are in agreement with the protonolysis of about two W−Cl moieties by silanols and formation of a mixture of bisiloxy, $[(\equiv SiO)_2WOCl_2]$ major species **1a** (ca. 80%) and monosiloxy $[(\equiv SiO)WOCl_3]$ minor species **1b** (ca. 20%) (Scheme 1).

Scheme 1. Grafting of $[WOCl_4]$ on SiO_{2-200}

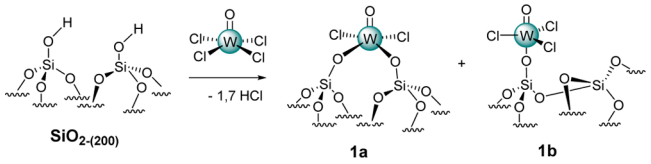

Characterization of **$WOCl_4$-SiO_{2-200}** was carried out further by a XAS study, which consisted in recording and analyzing the W L_{III}-edge extended X-ray absorption fine structure (EXAFS) spectra of the supported tungsten complexes resulting from the grafting of $[WOCl_4]$ on SiO_{2-200}.

For **$WOCl_4$-SiO_{2-200}**, the parameters obtained from the fit of the $k^3.\chi(k)$ EXAFS signal are consistent with the following coordination sphere around W (Figure 2 and Table 1): one oxygen atom at 1.68(1) Å, assigned to an oxo ligand, a bit less than two oxygen atoms (1.7 ± 0.3 O) at 1.87(1) Å, corresponding to σ-bonded siloxy ligands and a bit more than two chloride centers (2.3 ± 0.3 Cl) at 2.30(1) Å. This is consistent with the bond distances found in $[OWCl_2(OAr)_2]$, a type of molecular complexes where the W═O (1.638−1.715 Å), W−O (1.831−1.978 Å), and W−Cl (2.309−2.383 Å) bond lengths are in the same range.[13−20] Similar W−Cl bond distances have also been observed for crystalline $WOCl_4$ (2.28 Å for W−Cl; 1.8 Å for W═O)[21] or for molecular complexes where $WOCl_4$ is bonded to azoxybenzene[22] (2.279 to 2.308 Å for W−Cl; 1.651 to 1.687 Å for W═O) or to a ketone,[23] $CF_3C(O)CH{=}CHNHC_6H_5Br$ (2.259 to 2.308 Å for W−Cl; 1.664 Å for W═O). Similar parameters were obtained when fitting the $k^2.\chi(k)$ spectrum. The results thus agree with a major bis-siloxy structure, $[(\equiv SiO)_2WOCl_2]$ **1a** (70−80%), along with the monosiloxy species, **1b** (20−30%). This result is supported by NMR of the sample $[WOCl_4]$ on SiO_{2-200} selectively enriched on the oxo moiety by ^{17}O NMR (see below).

To gain further insights on the above-described experimental data, DFT calculations were carried out to confirm and refine the understanding of the grafting reaction of $[WOCl_4]$ onto silica dehydroxylated at 200 °C (SiO_{2-200}). In the continuation of previous theoretical studies,[7,24−28] we considered as surface models three polyoligosilsesquioxane derivatives: monosilanol **c**, and bis-silanols **b** and **ac**, with differing connectivity between the two SiOH groups (Figure 3). These models are suitable for isolated (model **c**) and for vicinal silanol groups (models **b** and **ac**). Thus, **c** accounts for highly dehydroxylated SiO_{2-700} surface, whereas **c**, **b**, and **ac** represent the various configurations for the SiO_{2-200} surface.

The grafting reaction was thus studied using these models. Full detailed studies available in the Supporting Information describe the reaction of $[WOCl_4]$ with the three silica models. In the case of the vicinal silanols models **b** and **ac**, this includes a first study of a monografting step, that yields a $[(\equiv SiO)WOCl_3]$ species in proximity to a free silanol. In agreement with experimental results, silanolysis of the W−Cl bond is calculated to proceed efficiently by coordination of the surface silanol onto the tungsten center followed by HCl elimination. To summarize, the nature of the silanol group has a great influence on the geometry and stability of the grafted complex. As expected, the type of silanol at the silica surface determines the grafting mode of $[WOCl_4]$. Indeed, the presence of isolated silanol groups leads to the formation of monografted complexes, whereas the presence of vicinal silanol groups induces the formation of bisgrafted species (in this case the monografted species evolves into the bisgrafted one by reaction with the neighboring silanol). In the case of vicinal silanols, contrary to what was observed for group 4 metals neopentyl (Np) derivatives,[28] the reaction does not stop at the monosiloxy stage and proceeds to formation of bigrafted species. Furthermore, the flexibility of the vicinal anchoring site is also a key factor that dictates the structure of the resulting isomers.

Figures 4 and 5 represent the optimized structures for mono- and bisgrafted species, respectively. Calculated bond lengths are in the same range as those observed with EXAFS (see Table S1). Their relative energy indicates a significant preference for the square pyramidal coordination sphere, with the oxo moiety in the apical position, for both **1a** and **1b** species, as in $[WOCl_4]$. Two types of isomers for **1a** are accessible, with siloxy ligands in cis ($\mathbf{1a}_{ac\text{-}1}$, Figure 5a, and $\mathbf{1a}_{b\text{-}1}$, Figure 5d) or trans ($\mathbf{1a}_{ac\text{-}2}$, Figure 5b, and $\mathbf{1a}_{b\text{-}2}$ Figure 5e) configuration, with a higher stability for the cis configuration (in the chosen nomenclature, for instance $\mathbf{1a}_{ac\text{-}1}$ refers to a calculated structure

dx.doi.org/10.1021/cs501294j | ACS Catal. 2014, 4, 4232−4241

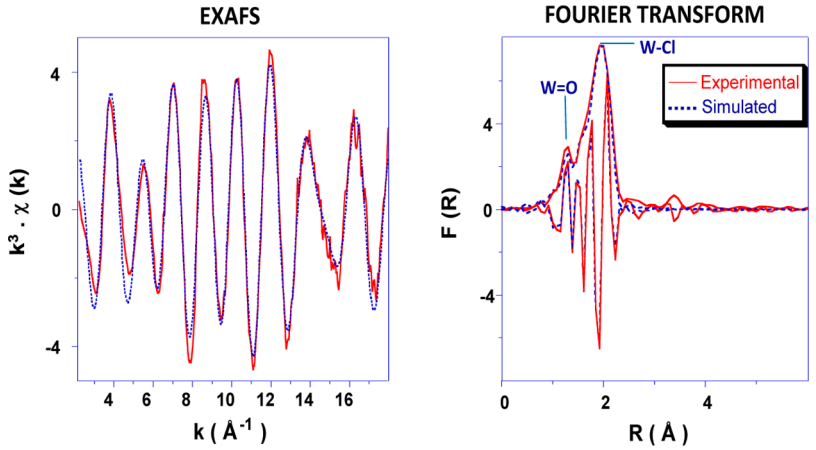

Figure 2. Tungsten L_{III}-edge k^3-weighted EXAFS (left) and corresponding Fourier transform (right, modulus and imaginary part) with comparison to simulated curves for **$WOCl_4$-SiO_{2-200}**. Solid lines: experimental; dashed lines: spherical wave theory.

Table 1. EXAFS Parameters Obtained for $WOCl_4$-SiO_{2-200}.[a]

type of neighbor	number of neighbors	distance (Å)	σ^2 (Å^2)
W=O	1.0	1.68(1)	0.0012(6)
W-OSi≡	1.7(3)	1.87(1)	0.0014(8)
W-Cl	2.3(3)[b]	2.30(1)	0.0036(6)

The errors generated by the EXAFS fitting program "RoundMidnight" are indicated in parentheses. [a]Δk: [2.1−18.0 Å^{-1}] - ΔR: [0.7−2.4 Å]; S_0^2 = 0.94; ΔE_0 = 9.5 ± 2.0 eV (the same for all shells); Fit residue: ρ = 4.1%; Quality factor: $(\Delta\chi)^2/\nu$ = 3.85, with ν = 11/19. [b]Shell constrained to the parameter above.

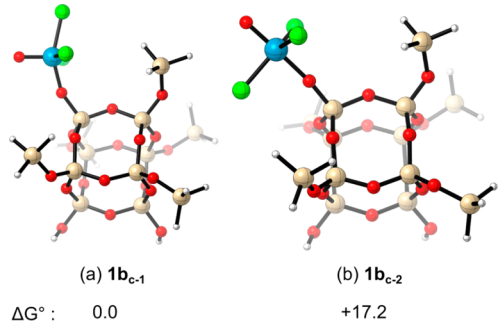

Figure 4. Optimized structures of complexes resulting from the grafting of [$WOCl_4$] on an isolated silanol group (**c** model). Δ*G*: relative Gibbs free energy of the different isomers (kcal mol^{-1}). Atom color code: blue: W; red: O; green: Cl; pale brown: Si; white: H.

of species **1a** built with an **ac**-type silica model). The isomers featuring a trigonal bipyramidal coordination type (**1a**$_{ac-3}$, Figure 5c, and **1**$_{ab-3}$, Figure 5f) are significantly less stable.

Having established preferred structural types as potential surface species from theoretical calculations, a further step would be to correlate such results to experimental evidence and reach a higher degree of understanding, beyond that accessible through the above-described techniques (IR and EXAFS, mostly).

We have previously demonstrated in related systems that ^{17}O NMR can afford most valuable structural information on oxo surface species, thanks inter alia to diagnostic quadrupolar and chemical shift anisotropic features.[7,29] These informative NMR parameters, when combined with DFT calculations, can afford access to structural data. We therefore proceeded to preparation of ^{17}O-labeled **$WOCl_4$-SiO_{2-200}** (**WO^*Cl_4-SiO_{2-200}**) for ^{17}O NMR studies. ^{17}O-enriched [$WOCl_4$] (designated as [WO^*Cl_4]) was prepared by treatment of [WCl_6] by 1 equiv of ^{17}O-labeled $Me_3SiO^*SiMe_3$ (obtained through hydrolysis of Me_3SiCl with 90%-^{17}O-enriched water).[30] Enrichment of the molecular precursor was confirmed by ^{17}O MAS NMR, as the spectrum comprises a single pattern that indicates the presence of a single site with isotropic chemical shift (CS) of 671 ppm (Figure S4). The sideband manifold results chiefly from chemical shift anisotropy (CSA). Here the presence of satellite transitions allows for fine adjustment of further parameters, most precisely, of the quadrupolar coupling constant (C_Q) and the asymmetry parameter (η_Q). Table 2 gathers the extracted NMR parameters, and Figure S4 in Supporting Information illustrates the finer influence of quadrupolar coupling on the outermost side bands (See

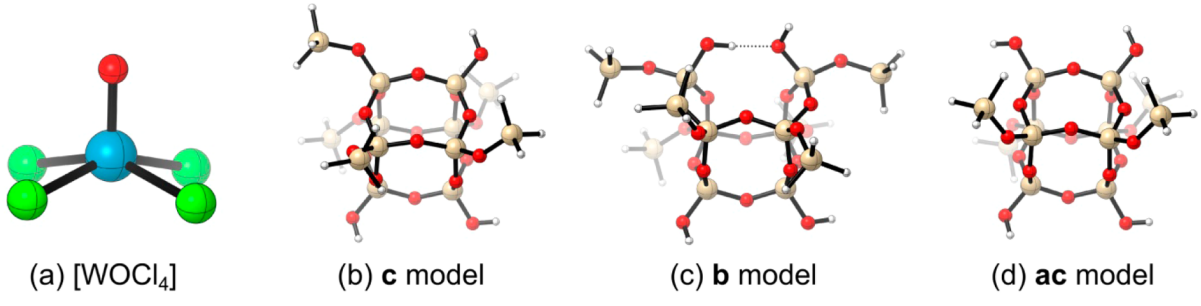

Figure 3. Optimized structures of (a) [$WOCl_4$] and of (b−d) the silanol models. Atom color code: blue: W; red: O; green: Cl; pale brown: Si; white: H.

dx.doi.org/10.1021/cs501294j | *ACS Catal.* 2014, 4, 4232−4241

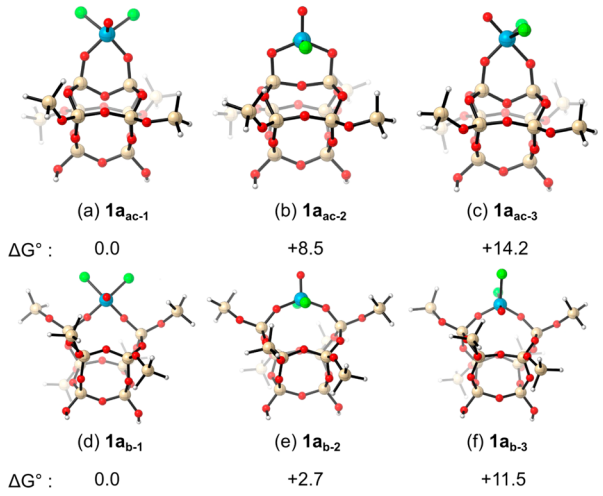

Figure 5. Optimized structures of complexes resulting from the bigrafting reaction of [$WOCl_4$] on vicinal silanol groups (**b** and **ac** models). ΔG: relative Gibbs free energy of the different isomers (kcal mol^{-1}). Atom color code: blue: W; red: O; green: Cl; pale brown: Si; white: H.

Table 2. Experimental and DFT-Calculated ^{17}O NMR Parameters for Mono- and Bigrafted Surface Species

		CS (ppm)	C_Q (MHz)	η_Q	Δ_{CSA} (ppm)	η_{CSA}
			[$WOCl_4$]			
exptl:		671	1.0	0.7	−330	0.6
DFT calcd:		708	0.3	0.01	−479	0.00
			bisgrafted species			
exptl:	**1a**	810	<2.5	nd[a]	−650	0.7
DFT calcd:	**1a**$_{ac-1}$	806	1.2	0.09	−496	0.07
	1a$_{ac-2}$	625	2.6	0.28	−584	0.74
	1a$_{ac-3}$	916	5.5	0.27	−719	0.21
	1a$_{b-1}$	798	1.4	0.26	−628	0.10
	1a$_{b-2}$	860	2.6	0.15	567	0.90
	1a$_{b-3}$	821	4.2	0.27	−591	0.20
			monografted species			
exptl:	**1b**	829	2.0	nd[a]	−350	1.0
DFT calcd:	**1b**$_{c-1}$	830	1.6	0.70	−626	0.25
	1b$_{c-2}$	923	5.9	0.02	−743	0.02

[a]Not determined.

Experimental Section for definitions). DFT calculations of [$WOCl_4$] ^{17}O NMR parameters have not been carried out on an isolated molecule, but they have been determined by taking into account the specific arrangement found in the crystal structure (See Supporting Information). As seen in Table 2, a good agreement is obtained for CS. Both C_Q and CSA values are in reasonable agreement with experimental features, considering the accuracy of their determination.

This compound was used for preparation of **WO*Cl$_4$-SiO$_{2-200}$** by reaction of [WO*Cl_4] with SiO_{2-200}. Furthermore, inspired by the conclusions drawn from EXAFS, that indicate presence of mono- and bisgrafted tungsten centers, we also prepared material **WO*Cl$_4$-SiO$_{2-700}$** from the reaction of [WO*Cl_4] with SiO_{2-700}. As this support features only noninteracting silanols, this will only comprise the monografted species [(≡SiO)WO*Cl_3] (**1b***). The ^{17}O MAS NMR spectrum of **WO*Cl$_4$-SiO$_{2-700}$** is displayed in Figure 6a. It features a pattern characteristic of a single site, at CS of 829

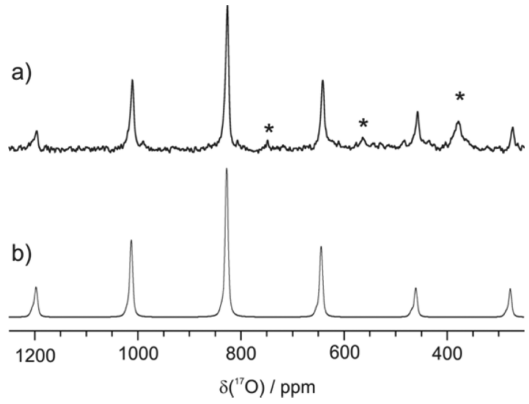

Figure 6. ^{17}O MAS NMR spectrum of **WO*Cl$_4$-SiO$_{2-700}$** at 18.8 T at a spinning speed of 20 kHz, number of scans: 16384 (a) together with best fit simulation (b). Asterisks designate the rotor's ZrO_2 signal.

ppm (cf. Table 2). Recording the spectrum at lower magnetic field (9.4 T) confirmed the small value of the quadrupolar coupling constant, as no broadening was detected (Figure S5). From best-fit simulations, an upper C_Q value of 2.0 MHz was determined.

From comparison with the DFT model species **1b**$_{c-1}$ and **1b**$_{c-2}$, experimental parameters (CS and C_Q, Table 2) are well in line with the former, namely, a square pyramidal coordination sphere, rather than trigonal bipyramidal, which allows us to conclude on the coordination geometry of the [(≡SiO)WO*Cl_3] **1b** surface species. One must also consider that the chemical shift anisotropy is not a discriminating parameter in this case.

The ^{17}O MAS NMR spectrum of **WO*Cl$_4$-SiO$_{2-200}$** recorded at 21.15 T (Figure 7a) results from overlapping of several components. Prior to further analysis, we have checked the origin of the signal broadening, which may be due to either large C_Q or to CS distribution.[29] Recording of the ^{17}O NMR

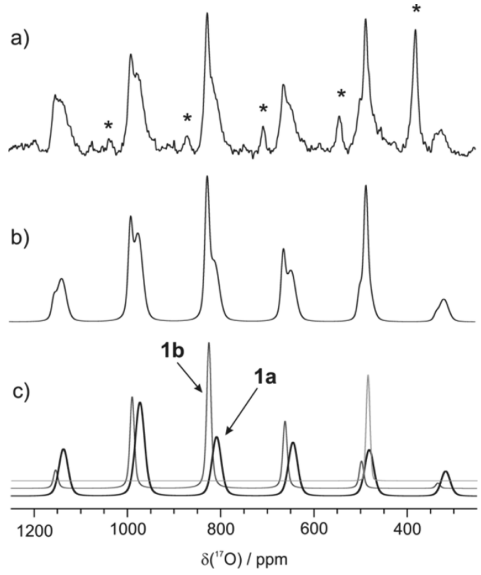

Figure 7. ^{17}O MAS NMR spectrum of **WO*Cl$_4$-SiO$_{2-200}$** at 21.15 T at a spinning speed of 20 kHz, number of scans: 114 688 (a) together with best fit simulation (b) and individual lineshapes for **1a** (black), **1b** (dark gray) and impurity (light gray) (c). Asterisks designate the rotor's ZrO_2 signal.

dx.doi.org/10.1021/cs501294j | ACS Catal. 2014, 4, 4232−4241

spectrum at lower field (9.4 T) affords a signal with comparable width (as expressed in ppm, see Supporting Information, Figure S6). This indicates that the width of the signal is mainly due to chemical shift distribution. The resulting best-fit simulation is presented in Figure 7b (see Table 2 for corresponding NMR parameters), and can be decomposed into three components, based on prior knowledge. As in our previous work, a Gaussian/Lorentzian line broadening of 1500 Hz was used to account for NMR parameters distribution.[7] One component at CS of 829 ppm with large CSA is identified as **1b** from comparison with data described above (Figure 6). It corresponds to a minor contribution of monografted species $[(\equiv SiO)WOCl_3]$ **1b** in **WO*Cl$_4$-SiO$_{2-200}$**, as already evidenced by EXAFS. A sharp signal at 480 ppm, featuring no CSA is also present, deduced from recording the spectrum at different MAS spinning speeds. The nature of the species accounting for less than 10% of the total signal is still unknown. Finally, the best fit simulation also includes a third component due to bigrafted species $[(\equiv SiO)_2WOCl_2]$ **1a***, present in dominant proportion. This site features a CS of 810 ppm, and it is characterized by large CSA (−650 ppm) and low C_Q (estimated to be less than 2.5 MHz), as determined by best fit simulation. In the case of supported species **1a**, that features large CSA and low C_Q, and where satellite transitions cannot be observed, the sideband manifold appears as dominantly affected by ^{17}O CSA. As no discontinuity appears in each individual band of the spectrum, only an upper value of quadrupolar coupling constant can be proposed from best-fit simulation (Table 2).

These values were compared with those of the DFT-optimized structures (Table 2). The combination of CS, C_Q, and CSA set of parameters allows for selection of **1a$_{ac\text{-}1}$** and **1a$_{b\text{-}1}$** as the closest candidates. Interestingly, they are also the most stable configurations in the series (Figure 5). The NMR lineshapes for all the calculated species (thus including **1a$_{ac\text{-}2}$**, **1a$_{ac\text{-}3}$**, **1a$_{b\text{-}2}$**, and **1a$_{b\text{-}3}$**) are presented in Figure S7. Their comparison further demonstrates the impact of the anisotropy onto the resulting signal and confirms our selection of models **1a$_{ac\text{-}1}$** and **1a$_{b\text{-}1}$**. Thus, we can conclude that surface species $[(\equiv SiO)_2WOCl_2]$ **1a** preferentially adopts a square pyramidal configuration (as in the case of **1b**), with cis siloxy moieties. The two DFT-calculated models (**1a$_{ac\text{-}1}$** and **1a$_{b\text{-}1}$**) illustrate the intrinsic heterogeneity of the SiO_{2-200} surface, which comprises unevenly spaced vicinal silanols: This translates into different SiO-W-OSi angles, but the W═O ^{17}O NMR parameters (CS, C_Q) are not significantly affected by this geometrical variation. This emphasizes the interest of probing the ^{17}O NMR parameters of the oxo group to unveil the nature of the first coordination sphere. From the best-fit simulation of the spectrum of **WO*Cl$_4$-SiO$_{2-200}$**, one can also estimate a relative proportion of 35/65 for mono versus bigrafted species. However, experimental uncertainties do not allow for non-ambiguous quantification, when relating this distribution to that obtained from elemental and mass-balance analyses, and from EXAFS.

Reactivity of WOCl$_4$-SiO$_{2-200}$ with (^{13}C-Labeled) SnMe$_4$. As mentioned in the introduction, previous elements indicate that use of tetra-alkyl tin derivatives is an efficient entry into the generation of metathesis active species from tungsten chloride precursors. We therefore attempted to generate surface alkyl derivatives using readily available tetramethyl tin as an alkylating agent. In order to ease spectroscopic investigations, we prepared ^{13}C-labeled $SnMe_4$, designated as $SnMe_4$*. The reaction of solid **WOCl$_4$-SiO$_{2-200}$** with a vapor pressure of $SnMe_4$* was performed at 80 °C during 12 h, generating material **WOMe*-SiO$_{2-200}$** as a brown material. All volatiles were transferred to an NMR tube fitted with a Young valve and containing C_6D_6. The resulting ^{13}C NMR spectrum displayed signals accounting for $SnMe_4$ (signal centered at −9.43 ppm with a $^1J(^{117/119}Sn-^{13}C)$ of 320.4/335.1 Hz), as well as for the expected Me_3SnCl side-product (−1.74 ppm with a $^1J(^{117/119}Sn\text{-}CH)$ of 360.1/377.4 Hz).[31,32] No signal to Me_2SnCl_2 was observed. The DRIFT spectrum of **WOMe*-SiO$_{2-200}$** (Figure 1c) displays new peaks compared to **WOCl$_4$-SiO$_{2-200}$**. Bands at 1455 and 1490 cm^{-1}, concomitant with the bands in the 2800 to 3000 cm^{-1} region, are characteristic of $\delta(C-H)$ and $\nu(C-H)$ respectively, accounting for methyl moieties. Moreover, the small amount of remaining isolated silanol groups is fully consumed after the alkylation, which can originate from reaction of $SnMe_4$ to afford $[(\equiv SiO)SnMe_3]$ species (vide infra).[33] The ^{1}H MAS NMR spectrum of **WOMe*-SiO$_{2-200}$** (Figure 8a) shows two broad signals around

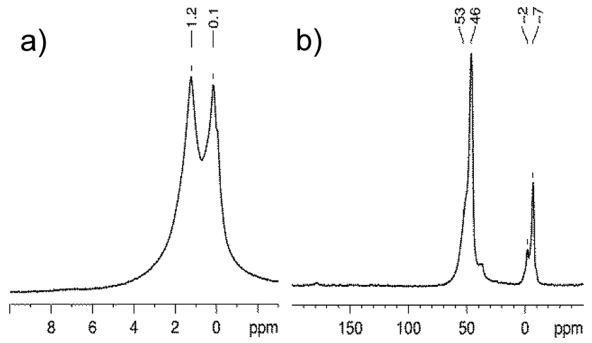

Figure 8. (a) ^{1}H MAS NMR spectrum of **WOMe*-SiO$_{2-200}$** (500 MHz, 8 scans, relaxation delay: 2 s, spinning speed: 10 kHz) (b) ^{13}C CP MAS NMR spectrum of **WOMe*-SiO$_{2-200}$** (125.7 MHz, 30 000 scans, relaxation delay: 2 s, CP contact time: 2 ms, spinning speed: 10 kHz) with 100% ^{13}C isotopic enrichment of the methyl carbon.

1.2 and 0.1 ppm, accounting for the methyl moieties bound on tungsten and tin, respectively. Similarly, the ^{13}C CP MAS spectrum features a sharp and intense signal at 46 ppm (Figure 8b), assigned to the characteristic W−Me fragment of $[(\equiv SiO)_2W(=O)Me_2]$, as observed in the closely related $[\{(t\text{-}Bu)_3SiO\}_2W(=O)Me_2]$ complex ($CS_{W\text{-}Me}$: 47.0 ppm).[34] Moreover, a shoulder at 53 ppm is also seen, which may arise from alkylation of monopodal species **1b**. In addition, peaks at −7 and −2 ppm are assigned to SnMe fragments on silica, as previously documented.[33] Formation of surface tin methyl species is probably due to reaction of $SnMe_4$ or $SnMe_3Cl$ (formed during the alkylation) with the remaining free silanol groups on the surface, as also observed by DRIFT.[33,35,36]

Further characterization of **WOMe-SiO$_{2-200}$** was carried out by EXAFS. Clearly, when compared to **WOCl$_4$-SiO$_{2-200}$**, the W−Cl scattering pathway decreases after alkylation (Figure 9). The parameters extracted from the fit of the $k^3\chi(k)$ EXAFS spectrum (Table 3) are consistent with one oxo ligand at 1.70(1) Å, ca. two oxygen atoms at 1.88(1) Å and three carbon atoms at 2.12(1) Å, respectively, assigned to siloxide and methyl ligands, consistently with the bond distances found in $[(Silox)_2(n\text{-}Bu)_2WO]$ (1.705(2) Å for W═O; 1.876 to 1.882 Å for W−O; 2.098 to 2.154 Å for W−C)[34] or in $(O\text{-}ArCH_2N(Me)CH_2Ar\text{-}O)(Me)_2WO$[37] (1.694−1.706 Å for

dx.doi.org/10.1021/cs501294j | ACS Catal. 2014, 4, 4232−4241

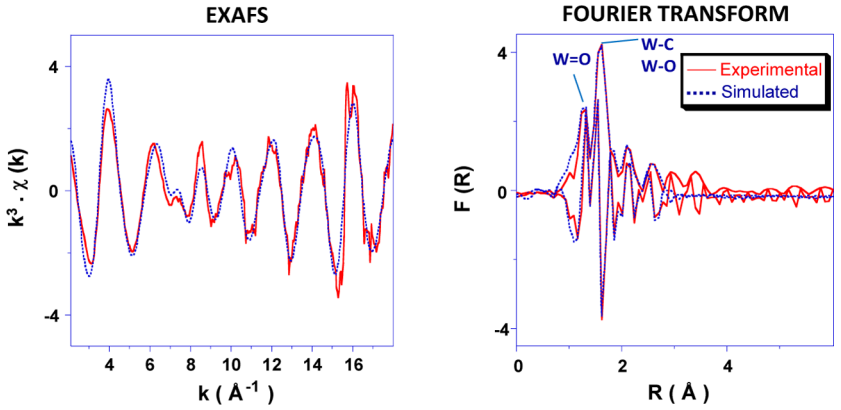

Figure 9. Tungsten L_{III}-edge k^3-weighted EXAFS (left), for **WOMe-SiO$_{2-200}$** and corresponding Fourier transform (right; modulus and imaginary part). Solid lines: experimental; dashed lines: spherical wave theory.

Table 3. EXAFS Parameters Obtained for WOMe-SiO$_{2\text{-}200}$[a]

type of neighbor	number of neighbors	distance (Å)	σ^2 (Å^2)
W=O	1.0	1.70(1)	0.0017(8)
W-OSi≡	1.8(2)	1.88(1)	0.0014(5)
W-CH_3	1.9(4)[b]	2.12(2)	0.006(4)
W-Cl	0.3(2)	2.36(2)	0.002(2)
W--O(Si≡)$_2$	1.0	2.91(3)	0.002(2)

[a]The errors generated by the EXAFS fitting program "RoundMidnight" are indicated in parentheses. Δk: [2.2 − 18.0 Å^{-1}] - ΔR: [0.7 − 2.9 Å] ([0.7 − 2.4 Å], when considering only the first coordination sphere without Cl); S_0^2 = 0.94; ΔE_0 = 8.7 ± 2.0 eV (the same for all shells); fit residue: ρ = 10.5%; quality factor: $(\Delta\chi)^2/\nu$ = 3.81, with ν = 11/24 ($[(\Delta\chi)^2/\nu]_1$ = 4.99 with ν = 11/19, considering only three backscatterers, oxo, −O, and −C, in the first coordination sphere of W). [b]Shell constrained to the parameters above and below.

W═O; 1.887 to 1.919 Å for W−O; 2.170 to 2.191 Å for W−C). The W−C distance obtained by EXAFS seems a bit short compared to the last example; however, W(O)−Me distances as short as 2.052 Å have already been reported.[38] Similar parameters were obtained when fitting the $k^2\chi(k)$ spectrum. Furthermore, the fit was improved by considering a further layer of Cl atom backscatterers at 2.37(2) Å (only ca. 0.3 such neighbors compared to 2.3 in the starting material), suggesting that the Cl/Me exchange may not be complete upon reaction with $SnMe_4$, and a layer of oxygen backscatterer at 2.91(4) Å which would be due to oxygen of surface siloxanes of silica. The results obtained are thus in good agreement with a Cl/Me exchange after the reaction of **WOCl$_4$-SiO$_{2-200}$** with $SnMe_4$ leading mainly to [(≡SiO)$_2$WOMe$_2$], with most probably [(≡SiO)WOMe$_2$Cl] as minor species (ca. 20−30%). This result is in accordance with ^{13}C CP NMR features that indicate the presence of minor monopodal W-Me containing species.

Catalytic Studies in Isobutene Metathesis. Exposure of 100 equiv of propene to **WOMe-SiO$_{2-200}$** at 150 °C in a batch reactor for 2 h led to the formation of equilibrated mixture of metathesis products: propene, ethene, and 2-butene (trans/cis ratio of 1.9, Figure S8), along with 0.9 equiv of methane per tungsten, in agreement with the formation of the expected carbenic catalytic active species [(≡SiO)WO(═CH$_2$)]. As reported in the literature in the case of monopodal [(≡SiO)(WO)Np$_3$], attempts to observe alkylidene species by heating (80 °C) prior to substrate addition were not successful.[5] The carbene ligand necessary for catalysis to proceed is probably generated in situ by α-H-transfer from a methyl ligand to generate a methylidene as active center.[39] Wolczanski described thermally stable complexes [(R$_3$SiO)$_2$WO$_2$R$_2$] that comprise trans siloxide fragments,[34] in a distorted trigonal pyramid geometry. In comparison, the peculiarity of the grafted system is the surface-enforced cis configuration of the siloxy groups, as demonstrated above by ^{17}O NMR combined DFT. This may have an impact on the formation of the carbene function by the α-H-transfer. However, further mechanistic studies would be necessary to elucidate this point.

The catalytic activity of **WOMe-SiO$_{2-200}$** was assessed in the self-metathesis of isobutene into ethylene and 2,3-dimethylbutenes (2,3-DMBs) (Scheme 2). The latter compounds are

Scheme 2. Isobutene Self-Metathesis

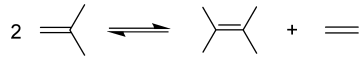

valuable additives for gasoline after a simple hydrogenation to 2,3-dimethylbutane with an impressive research octane number (RON) of 103.5 and low RVP (Reid vapor pressure).[40] 2,3-Dimethylbutenes are generally prepared by dimerization of propylene on nickel catalysts such as in the IFP Difasol process, which consist of a nickel salt in the presence of bulky basic phosphine dissolved in ionic liquid.[41] However, these processes are dependent on propylene, which has recently met increasing demand as starting material, resulting in a notable increase of its price.[42] Consequently, the development of a new approach to obtain 2,3-DMBs directly from alternative feeds, for example, readily available isobutene, is highly desirable.

Isobutene self-metathesis is rather challenging due to the less thermodynamically favored intermediate, as it bears *gem*-methyl substituents in the [1,2]-positions, generating a sterically encumbered intermediate. Productive metathesis of isobutene is thus disfavored for steric reasons which accounts for the relatively moderate activity observed in the conversion of isobutene in comparison to linear alkenes.[43] When isobutene self-metathesis is performed by using **WOMe-SiO$_{2-200}$** in a dynamic flow reactor (W = 7.10 wt %, T = 150 °C, P = 4 bar, total flow rate 10 mL·min^{-1} (50% isobutene in Ar)), the reaction proceeds with an initial maximal conversion of 9% (thermodynamic equilibrium at 12.5%) before reaching a pseudoplateau of 7% (Figure 10), affording a cumulated turn over number of 680 after 70 h. The product selectivities at the steady-state are branched hexenes (50%), ethene (49%) and

dx.doi.org/10.1021/cs501294j | ACS Catal. 2014, 4, 4232−4241

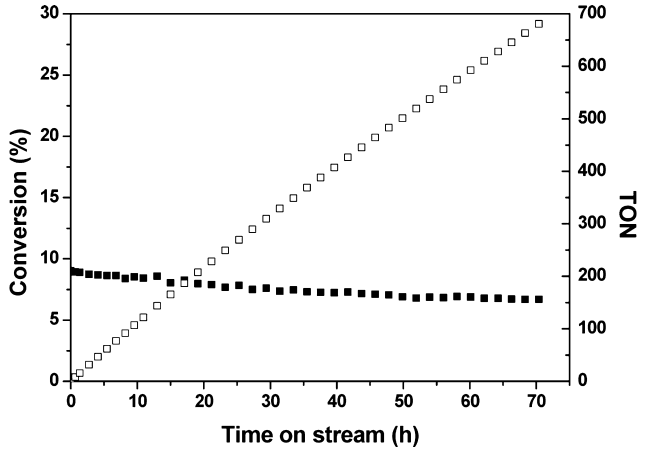

Figure 10. Conversion of isobutene catalyzed by **WOMe-SiO$_{2-200}$** (7.10 wt % W): (a) conversion of isobutene (■) and T.O.N (□).

diisobutenes (1%). The main hexenes component is 2,3-dimethyl-2-butene (DMB-2) with high relative selectivity (98%) obtained by self-metathesis of isobutene (Figure 11).

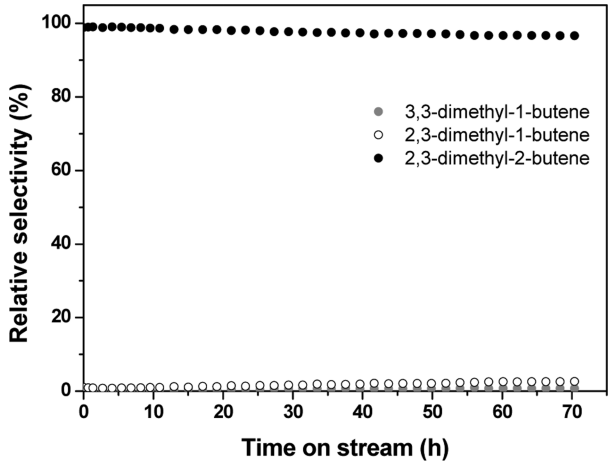

Figure 11. Relative selectivities in branched hexenes.

Very low selectivity toward DMB-1 (2%) results from DMB-2 isomerization. The present catalyst provides a second example for tungsten-based supported catalyst (apart from W−H/Al_2O_3) active in the highly challenging isobutene self-metathesis.[44,45]

CONCLUSION

The grafting of [$WOCl_4$] on SiO_{2-200} under controlled conditions was studied using experimental and theoretical approach. Combination of spectroscopic evidence backed up by DFT calculations demonstrated that the grafting results in bipodal tungsten oxo bischloride surface species [(≡SiO)$_2$$WOCl_2$] as the major component, along with minor monopodal tungsten oxo trischloride centers [(≡SiO)-$WOCl_3$]. ^{17}O NMR demonstrated that both these centers adopt a square pyramidal configuration, with the oxo ligand in apical position. Further treatment with $SnMe_4$ results in Cl/Me exchange within the surface species, as shown mainly by EXAFS and ^{1}H and ^{13}C MAS NMR. This material is active in alkene metathesis, achieving efficient conversion of the challenging isobutene substrate. Importantly, this catalyst shows high stability and selectivity toward ethylene and 2,3-dimethyl-2-butene. The reaction proceeds most probably by generation of bipodal tungsten oxo carbene species that resembles the proposed model for the industrial metathesis catalyst WO_3/SiO_2. Further studies will be devoted to the selective preparation and the characterization of such species and to the assessment of its catalytic performances.

EXPERIMENTAL SECTION

All experiments were carried out by using standard Schlenk and glovebox techniques. Solvents were purified and dried according to standard procedures. C_6D_6 (SDS) was distilled over Na/benzophenone and stored over 3 Å molecular sieves. ^{17}O-Enriched [$WOCl_4$] was prepared by using the reported procedure and 90% ^{17}O-labeled water.[30] 100% ^{13}C-labeled $SnMe_4$* was prepared from literature procedure, by alkylation of $SnCl_4$ using $^{13}CH_3MgCl$ in *n*-butylether.[46]

Propene (Air Liquide, 99.5%) was dried and deoxygenated before use by passing it through freshly regenerated molecular sieves (3 Å) and $R\bar{3}$−15 catalysts (BASF). Isobutene (Scott, 99%) was used as received. $SiO_{2-(200)}$ and $SiO_{2-(700)}$ were prepared from Aerosil silica (Degussa, specific area of 200 m^2 g^{-1}), which was partly dehydroxylated at 200 and 700 °C, respectively, under high vacuum (10^{-5} Torr) for 15 h to give a white solid having a specific surface area of 190 m^2 g^{-1} and containing 2.3 and 0.7 OH nm^{-2} respectively. Gas-phase analyses were performed on a Hewlett-Packard 5890 series II gas chromatograph equipped with a flame ionization detector and an Al_2O_3/KCl on fused silica column (50 m × 0.32 mm). Elemental analyses were performed at the Pascher Mikroanalytisches Labor at Remagen-Bandorf (Germany). IR spectra were recorded on a Nicolet 6700 FT-IR spectrometer by using a DRIFT cell equipped with CaF_2 window. The samples were prepared under argon within a glovebox. Typically, 64 scans were accumulated for each spectrum (resolution 4 cm^{-1}).

NMR Characterization. Solution NMR spectra were recorded on an Avance-300 Bruker spectrometer. All chemical shifts were measured relative to residual ^{1}H or ^{13}C resonances in the deuterated solvent: C_6D_6, δ 7.15 ppm for ^{1}H, 128 ppm for ^{13}C. ^{1}H and ^{13}C solid-state NMR spectra were recorded on a Bruker Avance-500 spectrometer with a conventional double-resonance 4 mm CP MAS probe at the Laboratoire de Chimie Organométallique de Surface. The samples were introduced under argon in a zirconia rotor (4 mm), which was then tightly closed. In all experiments, the sample was spun at 10 kHz unless otherwise specified. Chemical shifts were given with respect to TMS as external reference for ^{1}H and ^{13}C NMR. The ^{17}O solid-state NMR spectra were acquired on a Bruker Avance III 800 (^{1}H, 800.13 MHz; ^{17}O, 108.47 MHz) and 900 (^{17}O, 122.11 MHz) spectrometers. The ^{17}O MAS NMR spectra at 18.8 and 21.15 T were acquired using a single pulse sequence (pulse excitation of 2 μs at an RF field strength of 60 kHz) at spinning frequencies ranging from 17.6 to 20 kHz (3.2 mm rotor diameter) to avoid overlapping of spinning sidebands with CS resonances and to determine isotropic chemical shifts. No proton decoupling was applied. The recycle delay was 1 s.

Preparation and Characterization of $WOCl_4$-SiO_{2-200}. A mixture of finely ground [$WOCl_4$] (160 mg, 0.47 mmol) and SiO_{2-200} (1 g) was stirred at 80 °C (3h) under dynamic vacuum while all volatile compounds were condensed into a cold trap. Toluene was then added and the solid was washed 5 times. The resulting powder was dried under vacuum (10^{-5} Torr). Analysis

dx.doi.org/10.1021/cs501294j | ACS Catal. 2014, 4, 4232−4241

by infrared spectroscopy of the condensed volatiles indicated the formation of 674 μmol of HCl during the grafting for ca. 395 μmol of grafted tungsten (1.7 HCl/W). Elemental analysis: W 7.26 wt %; Cl 3.13 wt %(2.2 Cl/W).

Preparation and Characterization of WO*Cl$_4$-SiO$_{2-700}$. A mixture of finely ground 90% ^{17}O-labeled [WO*Cl$_4$] (120 mg, 0.35 mmol) and SiO$_{2-700}$ (1 g) were stirred at 80 °C (3h) under dynamic vacuum, while all volatile compounds were condensed into a cold trap. Toluene was then added, and the solid was washed 5 times. The resulting powder was dried under vacuum (10^{-5} Torr). Analysis by infrared spectroscopy of the condensed volatiles indicated the formation of 227 μmol of HCl during the grafting for ca. 245 μmol of grafted tungsten (0.9 HCl/W). Elemental analysis: W 4.5 wt %; Cl 2.71 wt % (3.1 Cl/W).

Alkylation of WOCl$_4$-SiO$_{2-200}$ with SnMe$_4$. One gram of material **WOCl$_4$-SiO$_{2-200}$** was exposed to SnMe$_4$ vapor pressure at 80 °C in a batch reactor. After 12 h, all volatile compounds were condensed into a NMR tube (fitted with a Young valve) containing C$_6$D$_6$. The resulting powder was dried under vacuum (10^{-5} Torr). ^{1}H MAS NMR (300 MHz) δ 0.1, 1.2 ppm. ^{13}C CP MAS NMR (75.4 MHz) δ 46, −2, −7 ppm. Elemental analysis: W 7.10 wt %; C 1.20 wt %; Sn 0.7 wt % (ca. 2.6 C/Wand 0.15 Sn/W).

Propene Metathesis. Twenty-five milligrams of **WOMe-SiO$_{2-200}$** was transferred to a 500 mL Schlenk flask in the glovebox. About 100 equiv (with respect to tungsten) of purified propene was then introduced into the flask and then heated to 150 °C from room temperature (heating rate: 4 °C/min). The gas-phase composition in the flask was determined by GC (HP 5890, 30 m × 0.32 mm KCl/Al$_2$O$_3$ column, FID).

Isobutene Metathesis. The evaluation of the activity of the catalyst **WOMe-SiO$_{2-200}$** in isobutene metathesis has been performed in a continuous flow reactor (Microactivity-Reference, PID Eng&Tech). The catalytic test were performed at 150 °C, with a flow rate of 10 mL·min^{-1} (5 mL·min^{-1} isobutene + 5 mL·min^{-1} argon), pressure = 4 bar, and 0.25 g of catalyst). Isobutene was introduced by a high pressure syringe (PMHP50−500, Top Industrie). The products were analyzed by online GC (Agilent 7890A) equipped with KCl/Al$_2$O$_3$ column and FID. The conversion and selectivity were calculated from carbon numbers.

SIMPSON Simulation of ^{17}O MAS NMR Spectra. All ^{17}O MAS NMR numerical spectra were calculated using *gcompute* method implemented in SIMPSON software package.[47] This package described each line shape with nine NMR interaction parameters, which included the isotropic chemical shift (δ_{CS}) defined in eq 1, the quadrupolar coupling constant (C_Q), and quadrupolar asymmetry parameter (η_Q) defined in eq 2 and eq 3, the CSA (Δ_{CSA}) and chemical shift asymmetry parameter (η_{CSA}) (in the Haeberlen convention) defined in eq 4 and eq 5, and the Euler angles (α, β, γ). Here the Euler angles were kept to zero due to the impossibility to assess them with the available experimental data sets. Each numerical simulation was performed with the zcw4180 crystallite file and 30 gamma angles, with the calculated FID inclusive of all quadrupolar satellites. A line broadening of 600, 800, and 1500 Hz was applied for simulated spectra of [WO*Cl$_4$], **WO*Cl$_4$-SiO$_{2-700}$** and **WO*Cl$_4$-SiO$_{2-200}$**, respectively, with Gaussian/Lorentzian ratio of 0.6.

$$\delta_{CS} = (\delta_{11} + \delta_{22} + \delta_{33})/3 \quad (1)$$

$$C_Q = e^2qQ/h = eV_{33}Q/h,\ |V_{33}| \geq |V_{22}| \geq |V_{11}| \quad (2)$$

$$\eta_Q = (V_{11} - V_{22})/V_{33},\ (1 \geq \eta_Q \geq 0) \quad (3)$$

$$\Delta_{CSA} = \delta_{zz} - (\delta_{xx} + \delta_{yy})/2 = 3\delta/2,\ |\delta_{zz} - \delta_{CS}| \geq |\delta_{xx} - \delta_{CS}| \geq |\delta_{yy} - \delta_{CS}| \quad (4)$$

with the reduced anisotropy, $\delta = \delta_{33} - \delta_{CS}$

$$\eta_{CSA} = (\delta_{yy} - \delta_{xx})/(\delta_{zz} - \delta_{CS}),\ (1 \geq \eta_{CSA} \geq 0) \quad (5)$$

DFT Methodological Details. All DFT calculations were performed with Gaussian 03.[48] Calculations were carried out at the DFT level of theory using the hybrid functional B3PW91.[49−54] Geometry optimizations were achieved without any symmetry restriction. Calculations of vibrational frequencies were systematically done in order to characterize the nature of stationary points. Gibbs free energies were obtained at P = 1 atm and T = 298.15 K within the harmonic approximation for frequencies. Stuttgart effective core potentials and their associated basis set were used for silicon and tungsten.[55] The basis sets were augmented by a set of polarization functions (ζd = 0.284 for Si and ζf = 0.823 for W). Hydrogen, chlorine, and oxygen atoms were treated with 6-31G(d,p) double-ζ basis sets.[56,57] The optimized structures were used for ^{17}O NMR calculations. These calculations were also performed using a higher Dunning's correlation consistent basis set cc-PVTZ for the oxygen atoms.[58,59] In all cases, among the various theories available to compute chemical shielding tensors, the Gauge Including Atomic Orbital (GIAO) method has been adopted for the numerous advantages it presents.[60−65] Typically, in order to compare our calculations with experimental values, ^{17}O chemical shielding has been converted to chemical shift using the usual equation: $\delta_{iso} = \sigma_{iso\ ref} - \sigma_{iso\ sample}$, where $\sigma_{iso\ ref}$ is the isotropic ^{17}O chemical shielding of the liquid water. In the continuation of our previous studies,[7] an internal reference is used for the calibration of the $\sigma_{iso\ ref}$ value: $\sigma_{iso\ ref}$ = 292.2 ppm. The ^{17}O quadrupolar coupling constant C_Q and the asymmetry parameter η_Q, which describes the interaction between nuclear quadrupolar moment of the oxygen nuclei with the electric field gradient (EFG) arisen at these sites, are calculated from the EFG tensor eigenvalues V_{11}, V_{22}, and V_{33}.

EXAFS. X-ray absorption spectra were acquired at the ESRF, using the Swiss-Norwegian beamline BM01B (proposal no. 01-01-905), at room temperature at the tungsten L_{III} edge, with a double crystal Si(111) monochromator detuned 70% to reduce the higher harmonics of the beam. The spectra were recorded in the transmission mode between 9.98 and 11.45 keV. The supported W sample was packaged within an argon-filled glovebox in a double airtight sample holder equipped with kapton windows. This type of cell has already been used and proved to be very efficient for air-sensitive compounds such as [(≡SiO)HfNp$_3$] species supported onto Aerosil silica(800) where the Hf−C contribution could be clearly distinguished from Hf−O by EXAFS.[66] The spectra analyzed were the results of four such acquisitions, and no evolution could be observed between the first and last acquisition. The data analyses were performed by standard procedures using in particular the program "Athena"[67] and the EXAFS fitting program "Round-Midnight",[68] from the "MAX" package, using spherical waves. The program FEFF8 was used to calculate theoretical files for phases and amplitudes based on model clusters of atoms.[69] The value of the scale factor, S_0^2 = 0.94, was determined from the k^2

dx.doi.org/10.1021/cs501294j | ACS Catal. 2014, 4, 4232−4241

and $k^3\chi(k)$ spectra of a reference compound, a sample of $[WO(CH_2tBu)_3Cl]$ complex diluted in BN and carefully mixed and pressed as a pellet (one oxo at 1.70(1) Å, three carbon atoms at 2.10(1) Å and one chlorine at 2.43(1) Å in the first coordination sphere, with three carbon atoms at 3.28(3) Å).[7] The refinements were performed by fitting the structural parameters N_i, R_i, σ_i and the energy shift, ΔE_0 (the same for all shells). The fit residue, ρ (%), was calculated by the following formula:

$$\rho = \frac{\sum_k [k^3\chi_{exp}(k) - k^3\chi_{cal}(k)]^2}{\sum_k [k^3\chi_{exp}(k)]^2} * 100$$

As recommended by the Standards and Criteria Committee of the International XAFS Society, the quality factor, $(\Delta\chi)^2/\nu$, where ν is the number of degrees of freedom in the signal, was calculated, and its minimization considered in order to control the number of variable parameters in the fits.

■ ASSOCIATED CONTENT

Supporting Information

Additional spectroscopic data, DFT calculations on the mechanistic aspects of the grafting reaction, and coordinates of DFT-optimized structures. This material is available free of charge via the Internet at http://pubs.acs.org.

■ AUTHOR INFORMATION

Corresponding Authors

*E-mail: mostafa.taoufik@univ-lyon1.fr.
*E-mail: laurent.delevoye@ensc-lille.fr.
*E-mail: regis.gauvin@ensc-lille.fr.
*E-mail: laurent.maron@irsamc.ups-tlse.fr.

Notes

The authors declare no competing financial interest.

■ ACKNOWLEDGMENTS

We thank the CNRS, the French Ministry of Research and Higher Education, and the Agence Nationale de la Recherche (ANR-12-BS07-0021-01, OXOCAT) for their generous support. Financial support from the TGIR RMN THC Fr3050 for conducting the research is gratefully acknowledged. ESRF is acknowledged for providing beamtime, as well as Prof. E. Le Roux (University of Bergen, Norway) and Hermann Emerich (ESRF) for their kind support during the XAS acquisition.

■ REFERENCES

(1) Mol, J. C. *J. Mol. Catal. A: Chem.* **2004**, *213*, 39−45.
(2) Grunert, W.; Feldhaus, R.; Anders, K.; Shpiro, E. S.; Minachev, K. M. *J. Catal.* **1989**, *120*, 444−456.
(3) Popoff, N.; Mazoyer, E.; Pelletier, J.; Gauvin, R. M.; Taoufik, M. *Chem. Soc. Rev.* **2013**, *42*, 9035−9054.
(4) Basset, J. M.; Psaro, R.; Roberto, D.; Ugo, R. *Modern Surface Organometallic Chemistry*; Wiley-VCH: Weinheim, 2009.
(5) Mazoyer, E.; Merle, N.; de Mallmann, A.; Basset, J.-M.; Berrier, E.; Delevoye, L.; Paul, J.-F.; Nicholas, C. P.; Gauvin, R. M.; Taoufik, M. *Chem. Commun.* **2010**, *46*, 8944−8946.
(6) Conley, M. P.; Mougel, V.; Peryshkov, D. V.; Forrest, W. P.; Gajan, D.; Lesage, A.; Emsley, L.; Coperet, C.; Schrock, R. R. *J. Am. Chem. Soc.* **2013**, *135*, 19068−19070.
(7) Merle, N.; Girard, G.; Popoff, N.; De Mallmann, A.; Bouhoute, Y.; Trebosc, J.; Berrier, E.; Paul, J. F.; Nicholas, C. P.; Del Rosal, I.; Maron, L.; Gauvin, R. M.; Delevoye, L.; Taoufik, M. *Inorg. Chem.* **2013**, *52*, 10119−10130.
(8) Rice, G. L.; Scott, S. L. *Langmuir* **1997**, *13*, 1545−1551.
(9) Demmelmaier, C. A.; White, R. E.; van Bokhoven, J. A.; Scott, S. L. *J. Phys. Chem. C* **2008**, *112*, 6439−6449.
(10) Popoff, N.; Espinas, J.; Goure, E.; Boyron, O.; Le Roux, E.; Basset, J. M.; Gauvin, R. M.; De Mallmann, A.; Taoufik, M. *Macromol. Rapid Commun.* **2011**, *32*, 1921−1924.
(11) van Roosmalen, A. J.; Polder, K.; Mol, J. C. *J. Mol. Catal.* **1980**, *8*, 185−190.
(12) Tosin, G.; Delgado, M.; Baudouin, A.; Santini, C. C.; Bayard, F.; Basset, J. M. *Organometallics* **2010**, *29*, 1312−1322.
(13) Gomez, F. J.; Manak, M. S.; Abboud, K. A.; Wagener, K. B. *J. Mol. Catal. A: Chem.* **2000**, *160*, 145−156.
(14) Lehtonen, A.; Sillanpaa, R. *Polyhedron* **2002**, *21*, 349−352.
(15) Lehtonen, A.; Sillanpaa, R. *Inorg. Chem.* **2004**, *43*, 6501−6506.
(16) Millar, A. J.; White, J. M.; Doonan, C. J.; Young, C. G. *Inorg. Chem.* **2000**, *39*, 5151−5155.
(17) Nayab, S.; Park, W.; Woo, H. Y.; Sung, I. K.; Hwang, W. S.; Lee, H. *Polyhedron* **2012**, *42*, 102−109.
(18) Nugent, W. A.; Feldman, J.; Calabrese, J. C. *J. Am. Chem. Soc.* **1995**, *117*, 8992−8998.
(19) Redshaw, C.; Elsegood, M. R. J. *Eur. J. Inorg. Chem.* **2003**, 2071−2074.
(20) Redshaw, C.; Humphrey, S. M. *Polyhedron* **2006**, *25*, 1946−1954.
(21) Hess, H.; Hartung, H. *Z. Anorg. Allg. Chem.* **1966**, *344*, 157−166.
(22) Bassi, I. W.; Scordamaglia, R. *J. Organomet. Chem.* **1975**, *99*, 127−134.
(23) Sergienko, V. S.; Abramenko, V. L.; Ilyukhin, A. B. *Zh. Neorg. Khim.* **1997**, *42*, 945−951.
(24) Del Rosal, I.; Gerber, I. C.; Poteau, R.; Maron, L. *J. Phys. Chem. A* **2010**, *114*, 6322−6330.
(25) Del Rosal, I.; Poteau, R.; Maron, L. *Dalton Trans.* **2011**, *40*, 11211−11227.
(26) Del Rosal, I.; Poteau, R.; Maron, L. *Dalton Trans.* **2011**, *40*, 11228−11240.
(27) Del Rosal, I.; Tschan, M. J. L.; Gauvin, R. M.; Maron, L.; Thomas, C. M. *Polym. Chem.* **2012**, *3*, 1730−1739.
(28) Popoff, N.; Espinas, J.; Pelletier, J.; Macqueron, B.; Szeto, K. C.; Boyron, O.; Boisson, C.; Del Rosal, I.; Maron, L.; De Mallmann, A.; Gauvin, R. M.; Taoufik, M. *Chem. Eur. J.* **2013**, *19*, 964−973.
(29) Merle, N.; Trebosc, J.; Baudouin, A.; Del Rosal, I.; Maron, L.; Szeto, K.; Genelot, M.; Mortreux, A.; Taoufik, M.; Delevoye, L.; Gauvin, R. M. *J. Am. Chem. Soc.* **2012**, *134*, 9263−9275.
(30) Gibson, V. C.; Kee, T. P.; Shaw, A. *Polyhedron* **1988**, *7*, 579−580.
(31) Verdonck, L.; van der Kelen, G. P. *J. Organomet. Chem.* **1966**, *5*, 532−536.
(32) Verdonck, L.; van der Kelen, G. P. *J. Organomet. Chem.* **1972**, *40*, 143−150.
(33) Legagneux, N.; de Mallmann, A.; Grinenval, E.; Basset, J. M.; Lefebvre, F. *Inorg. Chem.* **2009**, *48*, 8718−8722.
(34) Rosenfeld, D. C.; Kuiper, D. S.; Lobkovsky, E. B.; Wolczanski, P. T. *Polyhedron* **2006**, *25*, 251−258.
(35) Corma, A.; Navarro, M. T.; Renz, M. *J. Catal.* **2003**, *219*, 242−246.
(36) Samuel, P. P.; Shylesh, S.; Singh, A. P. *J. Mol. Catal. A: Chem.* **2007**, *266*, 11−20.
(37) Lehtonen, A.; Sillanpaa, R. *J. Organomet. Chem.* **2007**, *692*, 2361−2364.
(38) Stavropoulos, P.; Wilkinson, G.; Motevalli, M.; Hursthouse, M. B. *Polyhedron* **1987**, *6*, 1081−1087.
(39) Schrock, R. R. *Chem. Rev.* **2002**, *102*, 145−179.
(40) Hancsók, J.; Magyar, S.; Nguyen, K. V. S.; Keresztúry, L.; Valkai, L. *Pet. Coal* **2003**, *45*, 99−104.
(41) Olivier-Bourbigou, H.; Magna, L.; Morvan, D. *Appl. Catal., A* **2010**, *373*, 1−56.
(42) Plotkin, J. S. *Catal. Today* **2005**, *106*, 10−14.
(43) Szeto, K. C.; Mazoyer, E.; Merle, N.; Norsic, S.; Basset, J. M.; Nichoas, C. P.; Taoufik, M. *ACS Catal.* **2013**, *3*, 2162−2168.

(44) Garron, A.; Stoffelbach, F.; Merle, N.; Szeto, K. C.; Thivolle-Cazat, J.; Basset, J. M.; Norsic, S.; Taoufik, M. *Catal. Sci. Technol.* **2012**, *2*, 2453−2455.
(45) Merle, N.; Stoffelbach, F.; Taoufik, M.; Le Roux, E.; Thivolle-Cazat, J.; Basset, J. M. *Chem. Commun.* **2009**, 2523−2525.
(46) Edgell, W. F.; Ward, C. H. *J. Am. Chem. Soc.* **1954**, *76*, 1169−1169.
(47) Bak, M.; Rasmussen, J. T.; Nielsen, N. C. *J. Magn. Reson.* **2000**, *147*, 296−330.
(48) Frisch, M. J.; Trucks, G. W.; Schlegel, H. B.; Scuseria, G. E.; Robb, M. A.; Cheeseman, J. R.; Montgomery, J. A.; Jr., V., T.; Kudin, K. N.; Burant, J. C.; Millam, J. M.; Iyengar, S. S.; Tomasi, J.; Barone, V.; Mennucci, B.; Cossi, M.; Scalmani, G.; Rega, N.; Petersson, G. A.; Nakatsuji, H.; Hada, M.; Ehara, M.; Toyota, K.; Fukuda, R.; Hasegawa, J.; Ishida, M.; Nakajima, T.; Honda, Y.; Kitao, O.; Nakai, H.; Klene, M.; Li, X.; Knox, J. E.; Hratchian, H. P.; Cross, J. B.; Bakken, V.; Adamo, C.; Jaramillo, J.; Gomperts, R.; Stratmann, R. E.; Yazyev, O.; Austin, A. J.; Cammi, R.; Pomelli, C.; Ochterski, J. W.; Ayala, P. Y.; Morokuma, K.; Voth, G. A.; Salvador, P.; Dannen-berg, J. J.; Zakrzewski, V. G.; Dapprich, S.; Daniels, A. D.; Strain, M. C.; Farkas, O.; Malick, D. K.; Rabuck, A. D.; Raghavachari, K.; Foresman, J. B.; Ortiz, J. V.; Cui, Q.; Baboul, A. G.; Clifford, S.; Cioslowski, J.; Stefanov, B. B.; Liu, G.; Liashenko, A.; Piskorz, P.; Komaromi, I.; Martin, R. L.; Fox, D. J.; Keith, T.; Al-Laham, M. A.; Peng, C. Y.; Nanayakkara, A.; Challacombe, M.; Gill, P. M. W.; Johnson, B.; Chen, W.; Wong, M. W.; Gonzalez, C.; Pople, J. A. *Gaussian03*, revision B.05; Gaussian, Inc.: Wallingford, CT, 2003.
(49) Burke, K.; Perdew, J. P.; Wang, Y.. Electronic Density Functional Theory: Recent Progress and New Directions. In*Derivation of a Generalized Gradient Approximation: the PW91 Density Functional*;Dobson, J. F., Vignale, G., Mas, M. P., Eds.; Plenum: New York, 1998.
(50) Perdew, J. P. Electronic Structure of Solids. In*Unified Theory of Exchange and Correlation Beyond the Local Density Approximation*; Ziesche, P., Eschrig, H., Eds.; Akademie: Berlin, 1991.
(51) Perdew, J. P.; Burke, K.; Wang, Y. *Phys. Rev. B* **1996**, *54*, 16533−16539.
(52) Perdew, J. P.; Burke, K.; Wang, Y. *Phys. Rev. B* **1998**, *57*, 14999−14999.
(53) Perdew, J. P.; Chevary, J. A.; Vosko, S. H.; Jackson, K. A.; Pederson, M. R.; Singh, D. J.; Fiolhais, C. *Phys. Rev. B* **1992**, *46*, 6671−6687.
(54) Perdew, J. P.; Chevary, J. A.; Vosko, S. H.; Jackson, K. A.; Pederson, M. R.; Singh, D. J.; Fiolhais, C. *Phys. Rev. B* **1993**, *48*, 4978−4978.
(55) Kuchle, W.; Dolg, M.; Stoll, H.; Preuss, H. *Mol. Phys.* **1991**, *74*, 1245−1263.
(56) Harihara, P. C.; Pople, J. A. *Theor. Chim. Acta* **1973**, *28*, 213−222.
(57) Hehre, W. J.; Ditchfie, R; Pople, J. A. *J. Chem. Phys.* **1972**, *56*, 2257−2261.
(58) Davidson, E. R. *Chem. Phys. Lett.* **1996**, *260*, 514−518.
(59) Woon, D. E.; Dunning, T. H. *J. Chem. Phys.* **1993**, *98*, 1358−1371.
(60) Ditchfield, R. *Mol. Phys.* **1974**, *27*, 789−807.
(61) Dodds, J. L.; McWeeny, R.; Sadlej, A. J. *Mol. Phys.* **1980**, *41*, 1419−1430.
(62) Junk, P. C.; Steed, J. W. *J. Organomet. Chem.* **1999**, *587*, 191−194.
(63) London, F. *J. Phys. Radium* **1937**, *8*, 397−409.
(64) McWeeny, R. *Phys. Rev.* **1962**, *126*, 1028−1034.
(65) Wolinski, K.; Hinton, J. F.; Pulay, P. *J. Am. Chem. Soc.* **1990**, *112*, 8251−8260.
(66) Tosin, G.; Santini, C. C.; Taoufik, M.; De Mallmann, A.; Basset, J. M. *Organometallics* **2006**, *25*, 3324−3335.
(67) Ravel, B.; Newville, M. *J. Synchrotron Rad.* **2005**, *12*, 537−541.
(68) Michalowicz, A.; Moscovici, J.; Muller-Bouvet, D.; Provost, K. *J. Phys. Conf. Ser.* **2009**, *190*, 012034.
(69) Ankudinov, A. L.; Ravel, B.; Rehr, J. J.; Conradson, S. D. *Phys. Rev. B* **1998**, *58*, 7565−7576.